

In silico characterization of a
cyanobacterial plant-type isoaspartyl
aminopeptidase/asparaginase

**Ronaldo Correia da Silva, Andrei Santos
Siqueira, Alex Ranieri Jerônimo Lima,
Adonis de Melo Lima, Alberdan Silva
Santos, et al.**

Journal of Molecular Modeling

Computational Chemistry - Life Science
- Advanced Materials - New Methods

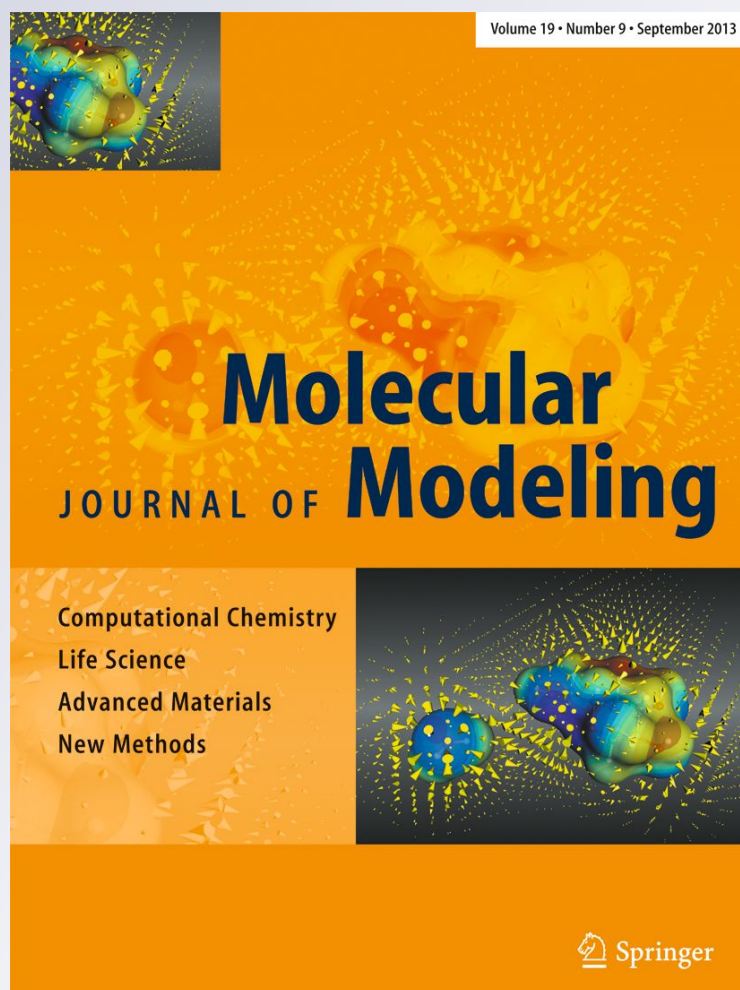
ISSN 1610-2940

Volume 24

Number 5

J Mol Model (2018) 24:1-10

DOI 10.1007/s00894-018-3635-6



Your article is protected by copyright and all rights are held exclusively by Springer-Verlag GmbH Germany, part of Springer Nature. This e-offprint is for personal use only and shall not be self-archived in electronic repositories. If you wish to self-archive your article, please use the accepted manuscript version for posting on your own website. You may further deposit the accepted manuscript version in any repository, provided it is only made publicly available 12 months after official publication or later and provided acknowledgement is given to the original source of publication and a link is inserted to the published article on Springer's website. The link must be accompanied by the following text: "The final publication is available at link.springer.com".



In silico characterization of a cyanobacterial plant-type isoaspartyl aminopeptidase/asparaginase

Ronaldo Correia da Silva¹ · Andrei Santos Siqueira¹ · Alex Ranieri Jerônimo Lima¹ · Adonis de Melo Lima¹ · Alberdan Silva Santos² · Délia Cristina Figueira Aguiar¹ · Evonnildo Costa Gonçalves¹

Received: 2 August 2017 / Accepted: 8 March 2018
© Springer-Verlag GmbH Germany, part of Springer Nature 2018

Abstract

Asparaginases are found in a range of organisms, although those found in cyanobacteria have been little studied, in spite of their great potential for biotechnological application. This study therefore sought to characterize the molecular structure of an L-asparaginase from the cyanobacterium *Limnothrix* sp. CACIAM 69d, which was isolated from a freshwater Amazonian environment. After homology modeling, model validation was performed using a Ramachandran plot, VERIFY3D, and the RMSD. We also performed molecular docking and dynamics simulations based on binding free-energy analysis. Structural alignment revealed homology with the isoaspartyl peptidase/asparaginase (EcAIII) from *Escherichia coli*. When compared to the template, our model showed full conservation of the catalytic site. In silico simulations confirmed the interaction of cyanobacterial isoaspartyl peptidase/asparaginase with its substrate, β -Asp-Leu dipeptide. We also observed that the residues Thr154, Thr187, Gly207, Asp218, and Gly237 were fundamental to protein–ligand complexation. Overall, our results suggest that L-asparaginase from *Limnothrix* sp. CACIAM 669d has similar properties to *E. coli* EcAIII asparaginase. Our study opens up new perspectives for the biotechnological exploitation of cyanobacterial asparaginases.

Keywords Comparative modeling · Molecular dynamics · Cyanobacteria · *Limnothrix* · Asparaginase

Introduction

Asparaginase (EC 3.5.1.1), glutaminase (EC 3.5.1.2), and glutaminase-asparaginase (EC 3.5.1.38) are aminohydrolases that catalyze the hydrolysis of asparagine (or glutamine) to aspartate (or glutamate) and ammonia. These enzymes play an important role in amino acid metabolism in a range of organisms. Additionally, they are of great biotechnological interest given their potential market and applications. L-asparaginase, for example, is a key component of therapy for acute lymphoblastic leukemia and other related blood cancers [1]; however, its effective clinical usage is complicated by

its significant glutaminase side activity [2]. L-asparaginase has also attracted the attention of the food processing industry as a promising acrylamide-mitigating agent [3].

Asparaginases constitute a diverse group of enzymes produced by microorganisms, plants, and animals, and include microbial L-asparaginases and plant L-asparaginases. Based on their amino acid sequences and structural and functional homology, microbial L-asparaginases can be divided into three types: (i) bacterial type L-asparaginases, (ii) plant-type L-asparaginases, also called type III, and (iii) enzymes similar to the thermolabile asparaginase from *Rhizobiummetli* [4].

Bacterial type L-asparaginases are further classified into types I and II according to their intra- or extracellular localization, substrate affinity, and oligomeric form [5]. Type I (cytosolic) have a low affinity for L-asparagine, while type II (periplasmic) have a high substrate affinity [6]. Bacterial type L-asparaginases catalyze the hydrolysis of the amide group of L-asparagine, producing L-aspartic acid and ammonia, while plant asparaginases and their bacterial homologs, plant-type asparaginases, hydrolyze the side-chain amide bonds of asparagine and isoaspartyl dipeptides, resulting in the release of L-Asp [5, 7].

✉ Ronaldo Correia da Silva
ronaldosilva@ufpa.br

¹ Laboratório de Tecnologia Biomolecular, Instituto de Ciências Biológicas (ICB), Universidade Federal do Pará (UFPA), Rua Augusto Correa, 01, CEP 66075-110, Guamá, Belém, Pará, Brasil

² Laboratórios de Investigação Sistemática em Biotecnologia e Biodiversidade Molecular, Instituto de Ciências Exatas e Naturais (ICEN), Universidade Federal do Pará (UFPA), Belém, Pará, Brasil

Plant and plant-type asparaginases form a subgroup of the N-terminal nucleophile (Ntn) hydrolase family that differ structurally from, and have a different evolutionary origin than, bacterial L-asparaginases [5]. They function as potassium-dependent or -independent Ntn hydrolases, similar to the well-characterized aspartyl glucosaminidases with ($\alpha\beta$)₂ oligomeric structure [5, 8, 9].

It should be taken into account that almost all of the enzyme modification experiments performed so far have been with L-asparaginases of *Eshcherichia coli* and *Erwinia* sp. A thorough exploration of the microbial world—a source of enzymes with various structural and functional properties—could lead to the discovery of more options for modifying L-asparaginase and for obtaining L-asparaginases with properties that better suit their usage in therapeutic and food processing applications [10]. To the best of our knowledge, data on cyanobacterial L-asparaginases are scarce. Thus, in this study, based on theoretical methods, we present the first structural characterization of a cyanobacterial plant-type L-asparaginase, as well as an evaluation of its substrate affinity in comparison to a homologous protein of *E. coli*.

Material and methods

Target sequence

The target nucleotide sequence in this study (GenBank ID: KEF43168.1) was obtained from a genomic analysis of the cyanobacterium *Limnothrix* sp. CACIAM 69d, which was isolated from a surface-water sample from the reservoir of the Tucuruí hydroelectric powerplant in Pará, Brazil (3°49'55"S, 49°38'50"W). The sequencing reads were obtained using a 454 GS FLX platform (Roche, Basel, Switzerland). After generating contigs, the unique bacterial-type II L-asparaginase open reading frame (ORF) was predicted by RAST [11]. Next, its relative nucleotide sequence was translated into an amino acid sequence by Geneious 7.0.4 (<http://www.geneious.com/>) using the bacterial genetic code. A BLASTX search [12] against the nr database corroborated the annotation of RAST.

Template selection and comparative modeling

The amino acid sequence (target) we obtained, which contained 324 residues, was submitted to the Protein Data Bank (PDB) server [13] in order to search for homologous structures. The best match we found was relative to an isoaspartyl aminopeptidase/asparaginase of *E. coli* (PDB:2ZAL), which was selected as the template. A member of the N-terminal nucleophile (Ntn) hydrolase family, this enzyme is expressed as inactive precursors that undergo activation in an autocatalytic manner. The subsequent maturation

process involves intramolecular hydrolysis of a single peptide bond, leading to the formation of two subunits (α and β) folded into one structural domain, with the nucleophilic Thr residue located at the free N-terminus of subunit β [5, 14].

Alignment of the target and template was performed using the ESPript 2.2 server [15]. Since the comparison of target and template indicated total structural conservation at the active site, similar to Michalska et al. [16], our study focused on the active site of the *Limnothrix* sp. CACIAM 69d enzyme.

MODELER v9.16 [17, 18] was used to build structural models. A total of 100 models were generated based on the target–template alignment, considering different conformations; they were then ranked by molecular probability density function (Molpdf) and DOPE score. After building a model, automatic loop refinement was used. The models were generated by satisfying spatial restrictions such as bond lengths, bond angles, dihedral angles, and interactions between non-bonded residues [19] before being subjected to validation. The stereochemical quality of each model was evaluated using a Ramachandran plot generated by the MolProbity server [20]. The quality of folding was determined by Verify3D [21] and the root mean square deviation (RMSD) [22] between the main chain of the template and the target was computed. Additionally, using the PBEQ-Solver server [23], we built an electrostatic potential map that revealed electrophilic and nucleophilic regions.

Molecular docking

Accordingly [24], we used the dipeptide β -Asp-Leu (code 2564466), which was retrieved from PubChem compound CID 3549397 [25], as a substrate. Gaussian 09 was employed to optimize and calculate the RESP charges of both ligands at the HF/6-31G* level of theory (Table 1) using the AMBER FF14SP force field. Docking simulations were done using the Molegro Virtual Docking 5 software [26]. The MolDock scoring function with a grid resolution of 0.30 was used to rank the solutions, toggling on Internal ES, Internal HBond, and Sp2-Sp2 torsions. The radius of the search area covered the key residues of previously described structural domains. Each docking involved 10 runs, a population size of 100, and a maximum of 2000 iterations.

Molecular dynamics simulation

The server H++ (<http://biophysics.cs.vt.edu/index.php>) was used to determine the protonation state of the protein at a pH of 7.0. All preparation and production steps in the MD simulation were performed with the AMBER 12 software [27]. The force field applied was FF14SB [28, 29].

The four systems were constructed—each with a ligand, Cl⁻ ions to neutralize the charges, and TIP3P water molecules [30]—in an octagonal box with dimensions of 10 Å in each

Table 1 Atom types and the RESP charges of the dipeptide L-Asp-L-Leu

Atom ID	Atom type	RESP charge
1	C1	0.013118
2	C2	-0.363301
3	C3	0.439820
4	H1	-0.003918
5	C4	0.704623
6	O1	-0.733686
7	O2	-0.733686
8	N1	-0.851078
9	C5	0.763077
10	O3	-0.644762
11	C6	-0.314016
12	C7	0.157137
13	H2	0.042117
14	C8	0.716639
15	O4	-0.721822
16	O5	-0.721822
17	N2	-0.303118
18	C9	0.018772
19	N3	-0.610077
20	C10	1.065995
21	N4	-1.056118
22	N5	-1.056118
23	H3	0.077569
24	H4	0.077569
25	H5	0.103520
26	H6	0.103520
27	H7	0.358799
28	H8	0.114635
29	H9	0.114635
30	H10	0.263027
31	H11	0.263027
32	H12	0.083682
33	H13	0.083682
34	H14	0.346797
35	H15	0.484684
36	H16	0.484684
37	H17	0.484684
38	H18	0.484684
39	H19	0.263027

direction of the protein. Energy minimization was performed in five steps; four of these steps each involved 3000 cycles of steepest descent and 5000 cycles of conjugate gradient, with the heavy atoms restrained by a harmonic potential of 1000 kcal/mol Å². In those four steps, we sequentially minimized (i) the hydrogen atoms in water molecules, (ii) the water molecules and ions, (iii) all hydrogen atoms, and (iv) the hydrogen atoms and water. In the last step (v), we used 5000 cycles of

steepest descent and 30,000 cycles of conjugate gradient and did not apply restraints. The heating and equilibration stage was divided into 14 steps. The temperature was gradually increased until it reached 300 K. Langevin dynamics (thermostat) were employed with a collision frequency of 3.0 ps⁻¹. A harmonic potential of 25 kcal/mol Å² was employed during the initial steps and was turned off at step 13. The heating procedure lasted 650 ps until step 13 and was performed using an NVT ensemble.

Afterwards, a 2-ns equilibration phase was employed in an NPT ensemble. The SHAKE algorithm was applied to constrain the vibrations of all bonds involving hydrogen atoms. The particle mesh Ewald method was used to calculate electrostatic interactions, with a cutoff value of 10.0 Å. 210 ns of MD simulation were carried out in an NVT ensemble for each system. The cpptraj module was used to compute the root mean square deviations (RMSDs) of both trajectories, considering the heavy atoms of the main chain.

Binding free-energy calculations

To calculate the binding free energies of the enzyme–substrate complexes, three methods were used: molecular mechanics generalized Born surface area (MM-GBSA), molecular mechanics Poisson–Boltzmann surface area (MM-PBSA) [31], and solvated interaction energy (SIE). These methods are classified as “final-stage” methods because they evaluate the energy difference between two end states of the system: bound and unbound.

MM-GBSA and MM-PBSA were implemented using the single trajectory protocol, calculated from each snapshot of the MD simulation with the receptor separated from the ligand, using implicit solvent molecular mechanics to calculate the free energy. These methods also permit a more accurate analysis of the contribution of each residue. It is also possible to decompose the interactions into different terms that describe the contributions of bonds, angles and dihedrals, electrostatic interactions, van der Waals interactions, and a solvation term that is decomposed into polar and nonpolar parts. The polar part can be calculated using the generalized Born method (MM-GBSA) or the Poisson–Boltzmann method (MM-PBSA). The nonpolar part is the energy needed for the solute to form a cavity within the solvent [19].

The binding free energy for a protein–ligand system calculated using PBSA/GBSA can be explored using the following equations:

$$\Delta E_{\text{MM}} = \Delta E_{\text{internal}} + \Delta E_{\text{electrostatic}} + \Delta E_{\text{vdw}} \quad (1)$$

$$\Delta G_{\text{ligand}} = G_{\text{complex}} - (G_{\text{ligand}} + G_{\text{receptor}}) \quad (2)$$

$$\Delta G_{\text{ligand}} = \Delta H - T\Delta S \approx \Delta E_{\text{MM}} + \Delta G_{\text{sol}} - T\Delta S \quad (3)$$

$$\Delta G_{\text{sol}} = \Delta G_{\text{(PB/GB)}} + \Delta G_{\text{SA}}, \quad (4)$$

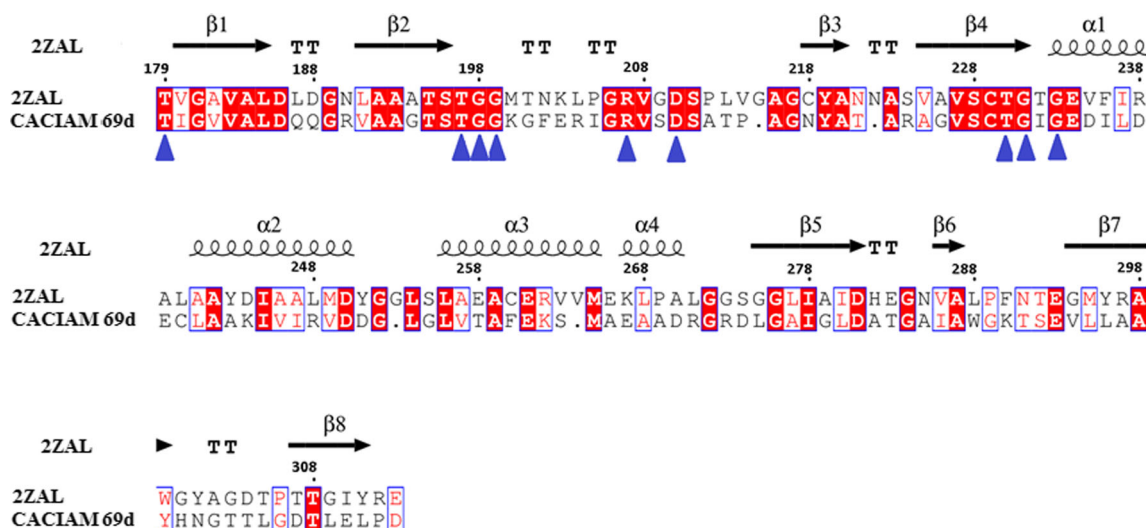


Fig. 1 Alignment between the target and template sequences (β -chains). The *blue arrows* point to the residues that make up the catalytic site. The *regions in red* represent the residues that have been conserved, and the *blue rectangles* highlight residues belonging to the same physicochemical group

where ΔG_{ligand} represents the binding free energy of the receptor and the ligand, ΔE_{MM} is the sum of the electrostatic interactions calculated in the gaseous phase, ΔG_{solv} is the desolvation free energy, $T\Delta S$ is the conformational entropy of the system, $\Delta E_{\text{internal}}$ is the total energy associated with the bonds, bond angles, and dihedrals in the molecules, $\Delta E_{\text{electrostatic}}$ is the electrostatic energy, E_{vdw} is the van der Waals energy term, and ΔG_{sol} is the sum of the

electrostatic ($\Delta G_{\text{(PB/GB)}}$) and non-electrostatic (ΔG_{SA}) components. Desolvation was calculated using implicit solvation models, such as the Poisson–Boltzmann (PB) and generalized Born (GB) models; these models vary in performance depending on the type of system considered [32].

The SIE was calculated from each snapshot of the MD simulation with the receptor separated from the ligand. The result is the sum of the intermolecular van der Waals interactions, Coulomb interactions, and the changes in the reaction energy field and nonpolar solvation energy. An entropy term was not explicitly included in the SIE. An empirical factor, α , was employed to predict the interaction free energy. This factor was obtained by analyzing 99 protein–ligand complexes, and it was included to compensate for the effect of the entropy on the free energy and thus ensure that the calculated results were close to the corresponding experimental values [20].

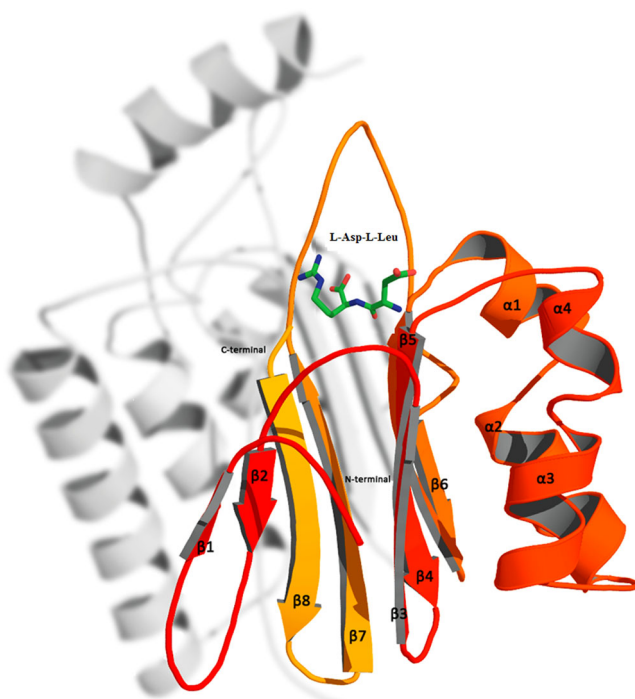


Fig. 2 α (translucent) and β (orange) chains of the cyanobacterium homology model with the substrate L-Asp-L-Leu complexed at the active site

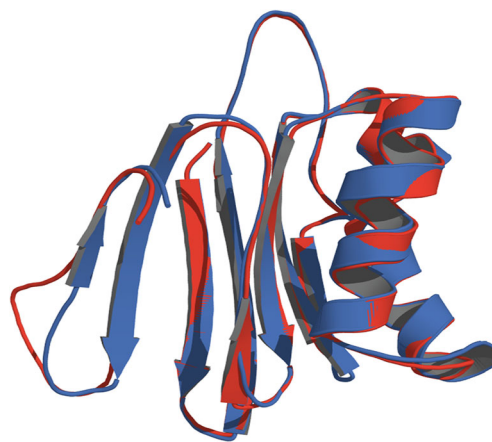


Fig. 3 Root mean square deviation (RMSD) between the target (*red*) and template (*blue*)

Results

Three-dimensional model of the isoaspartyl aminopeptidase/asparaginase of *Limnothrix* sp. CACIAM 69d

Alignment between the target and template sequences yielded 40% identity, 50% similarity, an e-value of 0.0, and an alignment score of 51,2174 (Fig. 1).

The three-dimensional model of the isoaspartyl aminopeptidase/asparaginase of *Limnothrix* sp. CACIAM 69d we obtained presented eight β -sheets and four α -helices (Fig. 2).

The Ramachandran plot showed that 93.5% of the residues were in energetically favorable regions, and the Verify3D analysis showed that 83.95% of residues had mean scores of at least 0.2, meaning that they were modeled well. Finally, superposition of the main chains ($C\alpha$ atoms) of the template and the target yielded a RMSD of 0.28 Å (Fig. 3), which corroborated the structural conservation observed in the target and template alignment sequences.

Molecular docking

Molecular docking was performed with the dipeptide substrate in both structures. Five poses were obtained after the docking run, and the best pose was selected according to the distance of the substrate from, its number of interactions with, and its affinity energy with the receptor (Tables 2, 3, and 4).

Molecular dynamics

MD simulation runs were performed for the target and template complexed with the dipeptide substrate. System stability was evaluated by calculating the RMSD. The template–substrate complex showed good stability in aqueous solution; the protein backbone presented RMSD values of around 1.5 Å. On the other hand, the target–substrate complex showed RMSD values of around 5 Å, probably because of its many loops. Nevertheless, after an initial period of variation, the system stabilized in terms of binding free energy, with the substrate remaining stable at the catalytic site (Fig. 4).

Table 2 Summary of docking poses of the dipeptide substrate in the target structure. The data for the best pose are shown in bold

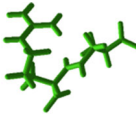
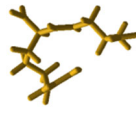
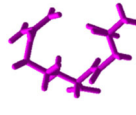
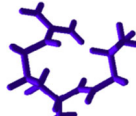
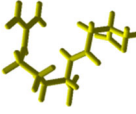
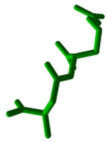

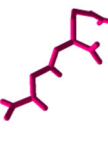
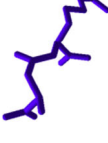
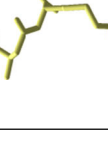
No	Pose 3D	MolDock Score	Rerank Score	Hbond
0		-105,108	-72,341	-7,798
1		-127,794	-89,236	-6,894
2		-109,295	-60,002	-6,717
3		-112,071	-63,599	-9,267
4		-101,653	-67,097	-5,748

Table 3 Summary of docking poses of the dipeptide substrate in the template structure 2ZAL. The data for the best pose are shown in bold

No	Pose 3d	MolDock Score	Rerank Score	Hbond
0		-129,696	-95,407	-11,260
1		-128,761	-101,876	-9,339
2		-127,665	-94,882	-7,222
3		-124,115	-90,051	-11,017
4		-123,086	-92,064	-5,959

The average distances of the two protein active-site residues from the dipeptide substrate during the 100-ns MD simulation, and corresponding experimental values, are presented in Table 5. The dipeptide substrate formed hydrogen bonds with the catalytic threonine that were $< 3 \text{ \AA}$ in length. Additionally, the residues Gly207 (199), Asp218 (210), and Gly237 (233) in the target (template) showed favorable distances from the substrate. The main finding of interest was that both the target and the template presented calculated distances of the substrate from the catalytic threonine that were shorter than the corresponding experimental values ($>3 \text{ \AA}$).

Table 4 Comparison between the energy scores of the best poses of the dipeptide substrate in the target and template structures

Template			Target		
MolDock	Rerank	HBond	MolDock	Rerank	HBond
-129,696	-95,407	-11,260	-105,108	-72,341	-7798

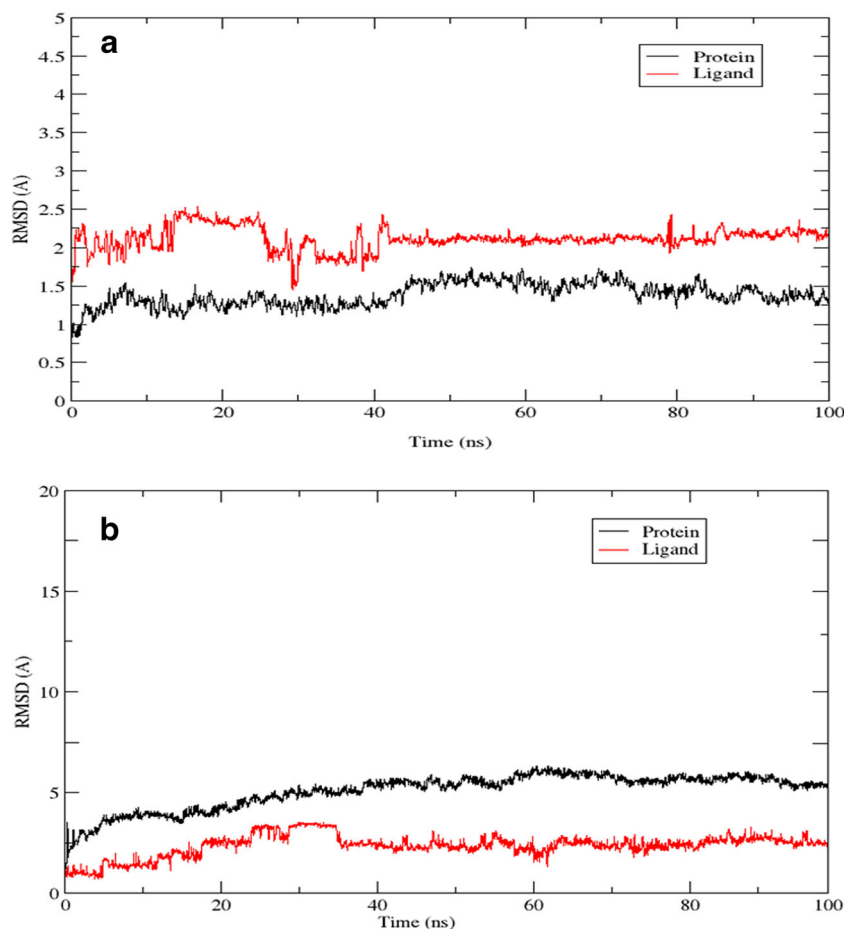
Binding free-energy calculations

The last 10 ns or 5000 frames of the MD simulation were used to perform binding free-energy calculations. The results afforded by the MM-GBSA, MM-PBSA, and SIE methods are presented in Table 6.

Discussion

Our first RAST annotation, confirmed by BlastX, indicated that the amino acid sequence we obtained was an asparaginase type 2. However, the functional identification we performed in the present study characterized our target as a plant-type isoaspartyl peptidase/asparaginase. L-asparaginase type 2-like enzymes present a conserved domain, i.e., the active site, which may affect the correct annotation of an open reading frame. Thus, our study reinforces the importance of theoretical analysis to refine the correct annotation of nucleotide sequences in genomic analysis [19, 33].

Fig. 4 a–b RMSD graphs of the template–substrate (**a**) and the target–substrate (**b**) complexes. The RMSD of the protein backbone is shown in *black*, and the RMSD of the ligand is shown in *red*



On the other hand, a structural comparison between *E. coli* EcAIII and *Limnothrix* sp. CACIAM 69d isoaspartyl peptidase/asparaginase revealed that there were no significant differences between their active sites after dipeptide substrate binding. Since the catalytic activity of the theoretical model from *Limnothrix* sp. CACIAM 69d could not be evaluated by homology

modeling alone, we also used molecular docking, molecular dynamics, electrostatic potential mapping, and binding free-energy tools to unravel the main function of this asparaginase: L-Asp-L-Leu dipeptide degradation. Similar results have been reported for other plant-type asparaginases, although they show higher affinities for isoaspartyl dipeptides [7, 14, 34].

Table 5 Average distances of the dipeptide substrate from atoms in the target and template

Residue of the target (template)	Protein...ligand interatomic distance considered	Average calculated value for distance in the target–substrate complex (Å)	Average calculated value for the distance in the template–substrate complex (Å)	Experimentally determined distance ^d (Å)
(N66)	HD2...O3	Not available	1.36 ^a	Not available
	H...O4	Not available	1.82 ^a	Not available
(R148)	OH...O5	Not available	2.11 ^a	Not available
T187 (179)	O...O2	2.43 ^a	2.21 ^a	>3 ^c
R215 (207)	N2...OH	2.97 ^a	2.59 ^a	Not available
T154	O...O2	2.49 ^a	Not available	Not available
G206 (199)	O...O2	2.67 ^a	2.58 ^a	>3 ^c
E207 (216)	OE2...O	2.80 ^a	2.37	Not available
D218 (210)	OD1...N2	2.91 ^a	>2.87 ^b	2.73 ^a

^a Hydrogen bond. ^b Hydrophobic interaction. ^c Induced dipole. ^d Experimentally determined distances for Asp [28]. The residues of interest in the template are shown in parentheses in the first column

Table 6 Summary of the binding free energy (ΔG_{bind}) values (in kcal mol⁻¹) calculated using the MM-PBSA, MM-GBSA, and SIE methods, as well as the standard deviation (SD) of and the standard error (SE) in each value

	MM-PBSA			MM-GBSA			SIE		
	ΔG_{bind}	SD	SE	ΔG_{bind}	SD	SE	ΔG_{bind}	SD	SE
Target	-24.5831	7.3951	2.2566	-24.8405	5.0070	0.1583	-6.07	0.06	0.29
Template	-29.4722	7.4008	0.2339	-30.1363	5.3162	0.1680	-6.46	0.03	0.42

A number of studies have shown that members of the Ntn hydrolase family utilize threonine as a nucleophile in dipeptide substrate cleavage [14, 16]. Similarly, *Limnothrix* isoaspartyl peptidase/asparaginase utilizes the Thr 187 residue, which is the essential catalytic residue. The residue Gly207 forms a hydrogen bond with the carboxyl group of the dipeptide substrate, thus keeping it close to the active site. Residues Asp218 and Gly233 form hydrogen bonds with the amine group of the substrate via side and main chains, respectively, providing fixation points for the substrate at the active site. Residues Arg207 and Asp218 also form hydrogen bonds with the side chain of the substrate [16].

Electrostatic interactions play an important role in biological systems [35–37]. In this study, it was observed that Thr154, Thr187, and Glu207 were crucial residues in the target system, while Asn66, Arg148, Thr179, and Glu216 were crucial residues in the template system. Both groups of residues interact electrostatically with the substrate, stabilizing it at the active site in preparation for nucleophilic attack by a threonine [16] (Tables 7 and 8).

Asparagine is an important nitrogen-donating metabolite in organisms [4], while aspartate is a precursor used in biosyntheses of other amino acids such as isoleucine, glycine, and serine. Thus, the enzyme isoaspartyl aminopeptidase/asparaginase, the focus of this study, may be involved in various metabolic paths related to growth and organism development [38, 39]. From a biotechnological perspective, aspartate is employed as a substitute for polyacrylate [40], which is nonbiodegradable, in the oil, paper, and paint industries [41]. Additionally, in cyanobacteria, isoaspartyl aminopeptidase/asparaginase is involved in the metabolism of cyanophycin, acts on the product of the degradation of cyanophycin by cyanophycinase, producing aspartates that may be used as biodegradable polymers which can substitute for polyacrylate in various applications [40]. Inhibiting isoaspartyl aminopeptidase/asparaginase along this path results in the accumulation of cyanophycin dipeptide, which is used as a natural additive in the pharmaceutical and food industries [42]. Also, optimizing the activity of isoaspartyl aminopeptidase/

Table 7 Results of binding free-energy decomposition based on the MM-GBSA method, focusing on the main residues in the target system

Residue	Van der Waals force (kJ mol ⁻¹)	Electrostatic interactions (kJ mol ⁻¹)	Polar interactions (kJ mol ⁻¹)	Nonpolar interactions (kJ mol ⁻¹)	Total energy (kJ mol ⁻¹)
Thr154	-0.95	-32.05	28.32	-0.16	-4.85
Thr187	-1.17	-0.42	-1.36	-0.19	-3.15
Gly207	0.37	-32.63	27.78	0.08	-4.55

Table 8 Results of binding free-energy decomposition based on the MM-GBSA method, focusing on the main residues in the template system

Residue	Van der Waals force (kJ mol ⁻¹)	Electrostatic interactions (kJ mol ⁻¹)	Polar interactions (kJ mol ⁻¹)	Nonpolar interactions (kJ mol ⁻¹)	Total energy (kJ mol ⁻¹)
Asn66	-1.22	-6.14	4.26	-0.20	-3.31
Arg148	0.46	-27.63	22.11	-0.12	-5.18
Thr179	0.08	-30.96	27.34	-0.11	-3.65
Glu216	0.87	-32.69	27.56	-0.13	-4.39

asparaginase could lead to improved aspartate production [42–44].

Conclusion

The present study is the first to characterize the functional structure of an asparaginase in a cyanobacterium, in this case *Limnothrix* sp. CACIAM69d. The model obtained shows high similarity to the *E. coli* asparaginase EcAIII, which is a plant-type asparaginase. This enzyme catalyzes the hydrolysis of both L-asparagine and isoaspartyl dipeptides formed during cell protein metabolism. The results we obtained support the hypothesis that the target structure has a similar function to that of the template. Future experiments should attempt to corroborate the catalytic function of cyanobacterial isoaspartyl aminopeptidase/asparaginase. Such experiments may include in silico and in vitro mutagenesis, an important strategy for exploring the biotechnological potential of cyanobacterial asparaginases.

Acknowledgements We acknowledge the financial support provided by the Fundação Amazônia de Amparo a Estudos e Pesquisas do Pará (FAPESPA): ICAAF 099/2014. The Conselho Nacional de Desenvolvimento Científico e Tecnológico (CNPq) also supported one of the authors (ECG) through grant 311686/2015-0.

References

- Shrivastava A, Khan AA, Khurshid M, Kalam MA, Jain SK, Singhal PK (2017) Recent developments in asparaginase discovery and its potential as anticancer agent. *Critic Rev Oncol/Hematol* 100:1–10
- Ln R, Doble M, Rekha VPB, Pulicherla KK (2011) In silico engineering of L-asparaginase to have reduced glutaminase side activity for effective treatment of acute lymphoblastic leukemia. *J Pediat Hematol/Oncol* 33(8):617–621
- Mohan Kumar NS, Shimray CA, Indrani D, Manonmani HK (2014) Reduction of acrylamide formation in sweet bread with L-asparaginase treatment. *Food Bioprocess Technol* 7(3):741–748
- Borek D, Jaskólski M (2001) Sequence analysis of enzymes with asparaginase activity. *Acta Biochim Pol* 48(4):893–902
- Michalska K, Jaskólski M (2006) Structural aspects of L-asparaginases, their friends and relations. *Acta Biochim Pol* 53(4):627–640
- Campbell HA, Mashburn LT, Boyse EA, Old LJ (1967) Two L-asparaginases from *Escherichia coli* B. Their separation, purification, and antitumor activity. *Biochemistry* 6(3):721–730
- Van Kerckhoven SH, de la Torre FN, Cañas RA, Avila C, Cantón FR, Cánovas FM (2017) Characterization of three L-asparaginases from maritime pine (*Pinus pinaster* Ait.). *Front Plant Sci* 8:1075
- Bruneau L, Chapman R, Marsolais F (2006) Co-occurrence of both L-asparaginase subtypes in *Arabidopsis*: At3g16150 encodes a K⁺-dependent L-asparaginase. *Planta* 224(3):668–679
- Credali A, Díaz-Quintana A, García-Calderón M, De la Rosa MA, Márquez AJ, Vega JM (2011) Structural analysis of K⁺ dependence in L-asparaginases from *Lotus japonicus*. *Planta* 234(1):109–122
- Krishnapura PR, Belur PD, Subramanya S (2016) A critical review on properties and applications of microbial L-asparaginases. *Crit Rev Microbiol* 42(5):720–737
- Aziz R, Bartels D, Best A, DeJongh M, Disz T, Edwards R, Formsma K, Gerdes S, Glass E, Kubal M, Meyer F, Olsen G, Olson R, Osterman A, Overbeek R, McNeil L, Paarmann D, Paczian T, Parrello B, Pusch G, Reich C, Stevens R, Vassieva O, Vonstein V, Wilke A, Zagnitko O (2008) The RAST server: rapid annotations using subsystems technology. *BMC Genomics* 9(1):75
- Altschul SF, Gish W, Miller W, Myers EW, Lipman DJ (1990) Basic local alignment search tool. *J Mol Biol* 215(3):403–410
- Berman HM, Westbrook J, Feng Z, Gilliland G, Bhat TN, Weissig H, Shindyalov IN, Bourne PE (2000) The Protein Data Bank. *Nucleic Acids Res* 28(1):235–242
- Michalska K, Brzezinski K, Jaskólski M (2005) Crystal structure of isoaspartyl aminopeptidase in complex with L-aspartate. *J Biol Chem* 280(31):28484–28491
- Gouet P, Courcelle E, Stuart DI, Métoz F (1999) ESPript: analysis of multiple sequence alignments in PostScript. *Bioinformatics* 15(4):305–308
- Michalska K, Hernandez-Santoyo A, Jaskólski M (2008) The mechanism of autocatalytic activation of plant-type L-asparaginases. *J Biol Chem* 283(19):13388–13397
- Šali A, Blundell TL (1993) Comparative protein modelling by satisfaction of spatial restraints. *J Mol Biol* 234(3):779–815
- Eswar N, Webb B, Marti-Renom MA, Madhusudhan MS, Eramian D, Shen M-Y, Pieper U, Sali A (2006) Comparative protein structure modeling using Modeller. *Curr Protoc Bioinformatics* Ch5: Unit5.6
- Martí Renom M, Stuart A, Fiser A, Sánchez R, Melo F, Šali A (2000) Comparative protein structure modeling of genes and genomes. *Annu Rev Biophys Biomol Struct* 29(1):291–325
- Hintze BJ, Lewis SM, Richardson JS, Richardson DC (2016) Molprobity's ultimate rotamer-library distributions for model validation. *Proteins* 84(9):1177–1189
- Eisenberg D, Lüthy R, Bowie JU (1997) VERIFY3D: assessment of protein models with three-dimensional profiles. *Methods Enzymol* 277:396–404
- Engh RA, Huber R (1991) Accurate bond and angle parameters for X-ray protein structure refinement. *Acta Crystallogr A* 47(4): 392–400
- Jo S, Vargyas M, Vasko-Szedlar J, Roux B, Im W (2008) PBEQ-Solver for online visualization of electrostatic potential of biomolecules. *Nucleic Acids Res* 36 (Suppl 2):W270–W275
- Larsen RA, Knox TM, Miller CG (2001) Aspartic peptide hydrolases in *Salmonella enterica* serovar Typhimurium. *J Bacteriol* 183(10):3089–3097
- Bolton E, Wang Y, Thiessen P, Bryant S (2008) Chapter 12—PubChem: integrated platform of small molecules and biological activities. *Annu Rep Comput Chem* 4:217–240
- Thomsen R, Christensen MH (2006) MolDock: a new technique for high-accuracy molecular docking. *J Med Chem* 49(11):3315–3321
- Case DA, Cheatham TE, Darden T, Gohlke H, Luo R, Merz KM, Onufriev A, Simmerling C, Wang B, Woods RJ (2005) The Amber biomolecular simulation programs. *J Comput Chem* 26(16):1668–1688
- Martí-Renom MASA, Fiser A, Sánchez R, Melo F, Sali A (2000) Comparative protein structure modeling of genes and genomes. *Annu Rev Biophys* 29:291–302

29. Field MJ, Albe M, Bret C, Proust-De Martin F, Thomas A (2000) The dynamo library for molecular simulations using hybrid quantum mechanical and molecular mechanical potentials. *J Comput Chem* 21(12):1088–1100
30. Price DJ, Brooks CL (2004) A modified TIP3P water potential for simulation with Ewald summation. *J Chem Phys* 121(20):10096–10103
31. Genheden S, Ryde U (2015) The MM/PBSA and MM/GBSA methods to estimate ligand-binding affinities. *Expert Opin Drug Discov* 10(5):449–461
32. Xu L, Sun H, Li Y, Wang J, Hou T (2013) Assessing the performance of MM/PBSA and MM/GBSA methods. 3. The impact of force fields and ligand charge models. *J Phys Chem B* 117(28):8408–8421
33. Chance MR, Bresnick AR, Burley SK, Jiang J-S, Lima CD, Sali A, Almo SC, Bonanno JB, Buglino JA, Boulton S, Chen H, Eswar N, He G, Huang R, Ilyin V, McMahan L, Pieper U, Ray S, Vidal M, Wang LK (2002) Structural genomics: a pipeline for providing structures for the biologist. *Protein Sci* 11(4):723–738
34. Cantor JR, Stone EM, Chantranupong L, Georgiou G (2009) The human asparaginase-like protein 1 hASRGL1 is an Ntn hydrolase with β -aspartyl peptidase activity. *Biochemistry* 48(46):11026–11031
35. Tasi G, Palinko I, Nyerges L, Fejes P, Foerster H (1993) Calculation of electrostatic potential maps and atomic charges for large molecules. *J Chem Inf Comput Sci* 33(3):296–299
36. Tasi G, Mizukami F (1998) Analysis of permanent electric dipole moments of aliphatic hydrocarbon molecules. 2. DFT results. *J Chem Inf Comput Sci* 38(2):313–316
37. Hong D-S, Cho SG (1999) Ab initio study of chlorosilanes: dipole moments and charge distributions. *J Chem Inf Comput Sci* 39(3):537–542
38. Azevedo RA, Lancien M, Lea PJ (2006) The aspartic acid metabolic pathway, an exciting and essential pathway in plants. *Amino Acids* 30(2):143–162
39. Hildebrandt Tatjana M, Nunes Nesi A, Araújo Wagner L, Braun H-P (2015) Amino acid catabolism in plants. *Mol Plant* 8(11):1563–1579
40. Schwamborn M (1998) Chemical synthesis of polyaspartates: a biodegradable alternative to currently used polycarboxylate homo- and copolymers. *Polym Degrad Stab* 59:39–45
41. Joentgen W, Groth T, Hai T, Oppermann-Sanio FB, Steinbu Èchel A (1998) Poster 51: Synthesis of poly- α -aspartic acid by hydrolysis of cyanophycin. In: *Int Symp on Biochemical Principles and Mechanisms of Biosynthesis and Biodegradation of Polymers*, University of Munster, Germany, 3–6 June 1998
42. Sallam A, Kast A, Przybilla S, Meiswinkel T, Steinbüchel A (2009) Biotechnological process for production of β -dipeptides from cyanophycin on a technical scale and its optimization. *Appl Environ Microbiol* 75(1):29–38
43. Sallam A, Steinbüchel A (2010) Dipeptides in nutrition and therapy: cyanophycin-derived dipeptides as natural alternatives and their biotechnological production. *Appl Microbiol Biotechnol* 87(3):815–828
44. Yagasaki M, Hashimoto S-I (2008) Synthesis and application of dipeptides; current status and perspectives. *Appl Microbiol Biotechnol* 81(1):13